

See discussions, stats, and author profiles for this publication at: <https://www.researchgate.net/publication/282330064>

# Shear Evolution of Fiberglass Composites Under Compression

Article in *Experimental Mechanics* · August 2015

DOI: 10.1007/s11340-015-0090-5

CITATIONS

2

READS

389

3 authors, including:



**Leslie Lamberson**

Colorado School of Mines

45 PUBLICATIONS 79 CITATIONS

[SEE PROFILE](#)



**Steven Pagano**

Drexel University

2 PUBLICATIONS 6 CITATIONS

[SEE PROFILE](#)

Some of the authors of this publication are also working on these related projects:



extreme composite behavior [View project](#)



NSF REU: Experiential Learning Undergraduate Research Opportunities on Energy and the Environment [View project](#)

# Shear Evolution of Fiberglass Composites Under Compression

L. Lamberson<sup>1</sup> · L. Shannahan<sup>1</sup> · S. Pagano<sup>1</sup>

Received: 18 July 2015 / Accepted: 26 August 2015  
© Society for Experimental Mechanics 2015

**Abstract** Woven composites can offer mechanical improvements over more traditional engineering materials, yet understanding the complex interplay between the fiber-matrix architecture during loading remains a challenge. This paper investigates the evolution of shear failure behavior during the compression of high performance fiberglass composites with varying resin binders at both quasi-static and dynamic strain rates. All samples are comprised of commercially available woven glass cloth with approximately 56 % fiber volume fraction. Laminates with thermosetting resin binders of silicone, melamine, and epoxy were examined. High-speed imaging reveals that failure occurs within a localized shear band region through multiple fiber-weave matrix interface failure with a characteristic macroscopic angle. The shear evolution was spatially mapped using grayscale histograms of the light intensity in the shear regions, and the resulting characteristic angles were measured and analyzed in the context of a Mohr-Coulomb failure criterion. Optical microscopy and high-speed imaging of the shear formation shows initiation appears due to local instabilities from kinking and microbuckling, influenced by the stacking and interlacing regions of tows.

**Keywords** Polymer matrix composites · Shear evolution · Compression · Instability · Cohesive strength · Internal friction

---

✉ L. Lamberson  
les@drexel.edu

<sup>1</sup> Drexel University, Philadelphia, PA 19106, USA

## Introduction

Polymer composite materials are being increasingly used in transportation, communication and defense applications due to their high strength-to-weight ratio and corrosion resistance, among other attractive properties. Unlike carbon fiber composites, fiberglass is electrically insulative and radiolucent (i.e. lacks a frequency signature) which is particularly suited for components in battery boxes, lightning exposed aircraft parts, missile casings, and other defense structures where conduction and radio-signal interference are avoided. As a result, investigating and characterizing fiberglass damage over a wide range of strain rates is critical as these materials are susceptible to high-velocity impact and/or explosion.

Under quasi-static loading in compression, shear, and tension, many types of polymeric composites have been extensively studied over the past couple of decades [1–11]. Under high strain rate loading, experimental configurations for impact testing of polymeric composites with gas-guns, drop-towers, Charpy tests, flyer impact, and Kolsky (split-Hopkinson) pressure bars have been explored, and are reviewed by Harding, Abrate, and Cantwell, to name a few [12–15]. Kumar et al. investigated unidirectional glass-epoxy composites with six different fiber orientations perpendicular to the axis of dynamic compressive loading, highlighting the coupled strain rate and orientation sensitivity [16]. Rate sensitivity up to  $10^2 \text{ s}^{-1}$  of unidirectional glass-epoxy composites was also demonstrated by Shokrieh, of cross-ply  $[0^\circ/90^\circ]$  composites by Ochola, and up to  $10^3 \text{ s}^{-1}$  of angled ply glass/epoxy laminates by Taab and Gilat [17–19]. Tay et al. examined cross-woven fiberglass reinforced with pure epoxy, as well as pure epoxy (by itself) under compression between  $5 \times 10^{-4}$  and

2500 s<sup>-1</sup>. They found that both epoxy alone, and the fiber reinforced epoxy demonstrated a dependence on strain rate and strain state, but one that decreased at higher rates. They also proposed a phenomenological expression to describe the stress-strain response for the composite [7]. The quasi-static and dynamic compressive behaviors of woven S-2 Glass/SC15 composite was investigated by Song et al., and a rate-sensitive empirical model of the constitutive response was presented [20]. Vural and Ravichandran examined uni-directional S-2 glass-epoxy composites under multi-axial compressive loading conditions from 10<sup>-4</sup> to 10<sup>4</sup> s<sup>-1</sup> and found the presence of shear bands shown in post-mortem SEM [21]. Khan et al. examined thick S2-glass woven laminates at various loading orientations, and determined that the failure stresses and strains in the ply lay-up direction were higher than those in the plane of the lamina [22]. El-Habak found a small rate sensitivity of woven fiberglass composites under impact loading [23]; whereas Weeks and Sun examined off-axis AS4/PEEK over a wide range of strain rates and determined the point where the composite exhibited nonlinear and strain rate dependent behavior [8]. Powers et al. examined Cycom 5920/1583 uniaxial E-glass cloth with rubber toughened epoxy composites at strain rates from 60 to 1150 s<sup>-1</sup> and determined that the ultimate strength did not significantly vary with strain rate, but the yield strength increased by a factor of 3.6 from low to high strain rates as the material transitioned from ductile to brittle behavior [24].

A glass woven fabric composite in an epoxy resin binder, most similar to those investigated in this study (commercially known as G10), was examined in and out-of-plane under dynamic compression by Nishida et al.. They demonstrated that this type of composite behaves in a nominally linear-elastic brittle fashion under dynamic compression, and were able to successfully demonstrate valid Kolsky (split-Hopkinson) results at uniform strain rate loading between 10<sup>2</sup> to 10<sup>3</sup> s<sup>-1</sup> using an optimized pulse shaping technique [25]. Ravi-Chandar and Satapathy also examined G10 and observed some nonlinear rate dependence attributed to the matrix, as well as finding that the material exhibited a two-fold increase in the compressive strength from quasi-static to dynamic compression [26]. The authors stated the loading rate was on the order of 10<sup>3</sup> s<sup>-1</sup> under dynamic conditions, but the specific value was difficult to obtain due to crumbling of the samples. They also noted cracking at approximately a 45 degree angle from the loading direction [26]. Neither of the studies on G10 provided *in-situ* visualization.

The constitutive response of polymeric composites under dynamic tensile loading were conducted by Harding and Dong, Benloulou et al. and Wang and Xia, among others, and have demonstrated a strain rate sensitive response [27–29]. A review of the large body of research on the

rate-effects of fiber reinforced composites can be found by Gresczuk and Sierakowski, Al-Hassani and Kaddour, among others [30–33]. It should be noted that while a significant amount of literature exists on the constitutive behavior of polymer matrix glass fiber composites, little to none have focused on systematic studies of similarly comprised woven composites with varying matrix materials that include *in-situ* visualization. Consequently, the focus in this study is to quantitatively examine the evolution of shear formation during quasi-static and dynamic compression of woven glass laminates with varying resin binders.

## Experimental Methods

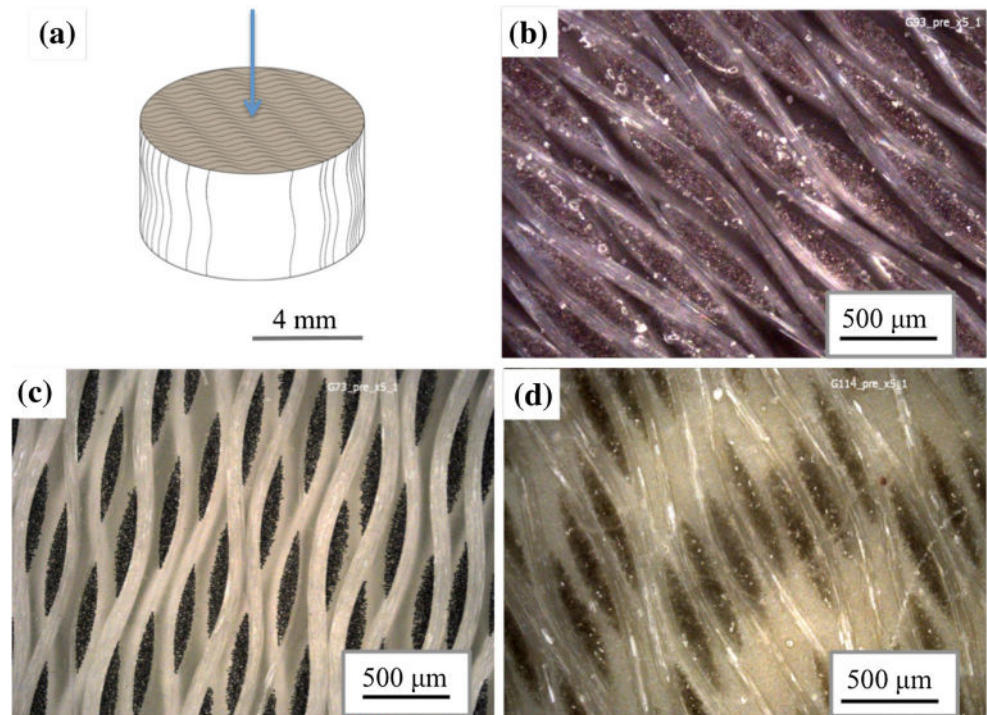
### Specimen Details

Three versions of commercially available woven glass cloth with nominally the same fiber volume fraction (approximately 56 % estimated from volume and weight measurements of the samples) were used for this study. Each composite varied in the type of thermosetting resin binder used in the matrix of either silicone, melamine, or epoxy (commercially G7, G9, and G11, respectively). Samples were cut between 5 to 7 mm long using a diamond-blade saw from vendor-supplied rods, and had a diameter of 8 mm ± 125 μm. Sample surfaces were lapped and polished to a finish of 3 μm in order to reduce friction between the platen-specimen interfaces during loading. Optical microscopy of the undamaged composites are shown in Fig. 1, along with a schematic of the loading orientation with respect to the weave for compression testing. Table 1 lists the composite densities, and individual binder material compressive strengths.

### Quasi-static Testing

All materials were subjected to uniaxial compression using a Shimadzu AG-IS frame with a 50 kN load cell at a strain rate of approximately 10<sup>-3</sup> s<sup>-1</sup>. To ensure alignment during testing and minimize unwanted shear forces, a specially-tailored aluminum ring is placed on the lower jacket with a concentric hole machined to the diameter of the steel platens used for testing. Once the sample has been accurately centered on the platen, the platen is placed on the jacketed compression plate using the ring, and the ring is carefully removed and used in the same manner to align the platen on the top plate. The platens are 12.5 mm diameter and approximately 3 mm thick steel, lapped and polished to a 3 μm finish. Silicone grease is used between the platen and loading surface to remove friction, and maintains enough tackiness to hold the upper platen in place during alignment.

**Fig. 1** (a) Schematic showing sample geometry and orientation of weave with respect to loading direction. Microstructure of woven glass fiber composites with (b) melamine resin binder, (c) silicone resin binder, and (d) epoxy resin binder



The surface between the sample and the platen is coated with a thin layer of Teflon spray and molybdenum powder to reduce friction. Before every test, a compliance test is performed to 45 kN. Tests were conducted in displacement control with a 50 N pre-load, loaded at a rate of 1 millimeter per minute. The force and displacement data is recorded by the load frame software at a sampling rate of 20 Hz.

### Dynamic Testing

The cylindrical specimens were loaded in compression using a Kolsky (split-Hopkinson) pressure bar to strain rates of approximately  $10^2$  to  $10^3$   $s^{-1}$  as show in Fig. 2. The bars have a diameter of 12.5 mm and are approximately 2.4 meters in length, made of C-350 maraging steel

**Table 1** Properties of three variants of glass fabric woven laminates investigated

Resin Binder	Density* (kg/m <sup>3</sup> )	Binder compressive Strength <sup>†</sup> (MPa)
Silicone	1808	61
Epoxy	1941	178
Melamine	1963	196

\*Measured in lab,  $\pm 10.3$  kg/m<sup>3</sup>

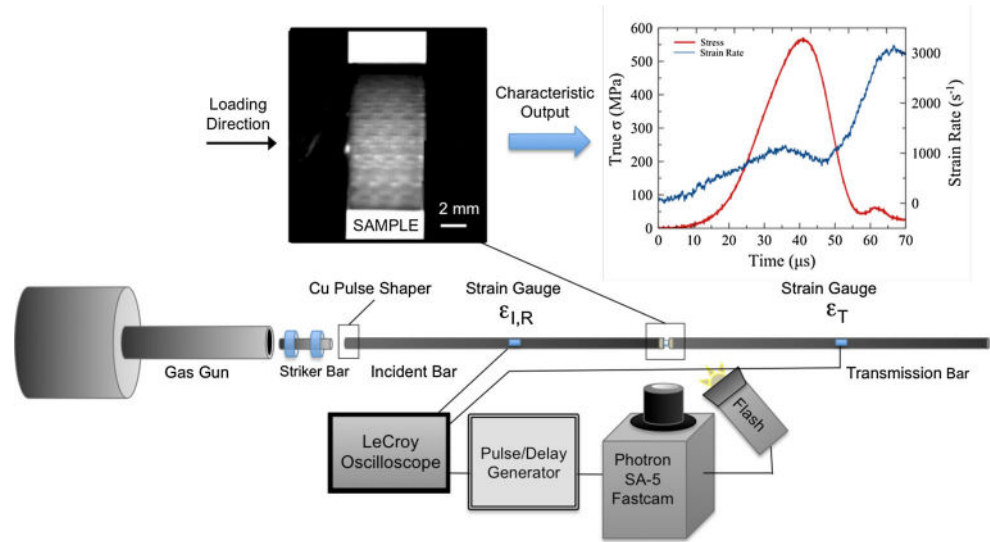
<sup>†</sup>From [34]

hardened to a yield stress of 2.68 GPa in order to remain elastic during a test. A 150 mm long striker of the same material is launched by means of a compressed nitrogen gas gun into the incident bar between 5 to 30 m/s. Annealed copper disks, as described by Frew et al. and Nishida et al. [25, 35, 36], approximately 4.22 mm in diameter and 0.6 mm in thickness were used to help more precisely control the profile of the incident pulse. Steel platens approximately 3 mm in thickness, polished to a 3  $\mu$ m finish, were placed between the sample and the bars to maintain an impedance match, yet shield the end of the bars from potential damage. Silicone grease was used between the specimen and the platens, and the platens and the bars to minimize interface friction.

The Kolsky technique is based on one-dimensional wave propagation theory and has been used to measure the dynamic compressive behavior of a wide variety of materials [37]. Data from strain gauges mounted in the center of the incident and transmissions bars are used to capture the response, and recorded using a LeCroy high definition 4024 oscilloscope with a 500 MHz bandwidth and 2.5 Gs/second sampling rate. The incident, reflected, and transmitted strain signals (or  $\varepsilon_I(t)$ ,  $\varepsilon_R(t)$ ,  $\varepsilon_T(t)$ , respectively) and are then used to obtain average stress and strain values, assuming the loading state in the sample is near uniform. Under these conditions, the signals are related by

$$\varepsilon_T(t) = \varepsilon_I(t) + \varepsilon_R(t) \quad (1)$$

**Fig. 2** Schematic of the Kolsky bar system with a characteristic woven glass fiber melamine resin binder composite shown, as well as the characteristic output of stress versus time and the strain rate during the test. After an initial  $10 \mu\text{s}$  rise time, the strain rate remains reasonably consistent around  $1000 \pm 250 \text{ s}^{-1}$  until macroscopic failure



and can be used, as commonly found in literature [38], to determine the nominal strain rate, strain and stress in the sample as

$$\dot{\varepsilon}(t) = -2\frac{c}{l_s}\varepsilon_R(t) \quad (2)$$

$$\varepsilon(t) = -2\frac{c}{l_s}\int_0^{t_f}\varepsilon_R(t)dt \quad (3)$$

$$\sigma(t) = \frac{EA}{A_s}\varepsilon_t(t) \quad (4)$$

where  $c$  represents the one-dimensional compression wave speed of the the bars (in our case experimentally measured as  $4890 \text{ m/s}$ ),  $E$  is the elastic modulus of the bars,  $l_s$  is the sample length, and  $A_s$  is the cross-section area of the sample, and  $A$  is the cross-section area of the bars as a function of loading time  $t_f$ . More details of this type of testing can be found in Ramesh, and Chen and Song [38, 39]. High-speed images were captured using a Photron SA-5 camera with a Sigma 105 mm lens at 262,500 frames per second (fps) with an exposure time of  $3.8 \mu\text{s}$ , and resolution of approximately  $100 \mu\text{m}/\text{pixel}$ . The samples were lit using a halogen flashbulb that is triggered from the launch of the striker such that it reaches a full illumination of  $1000 \text{ W}$  before the sample is loaded by the compression wave, and remains fully illuminated during the entirety of the loading pulse.

## Results and Discussion

The quasi-static compression behavior for representative tests for each resin binder material is presented in Fig. 3. The response is shown up to the point where there was a sudden significant drop in load carrying capability, at which point the specimen is considered to have macroscopically failed. The strength of the silicone resin binder woven glass

composite is  $134 \pm 3.5 \text{ MPa}$ , epoxy resin composites  $381 \pm 10.4 \text{ MPa}$ , and melamine resin composite at  $484 \pm 13.2 \text{ MPa}$ . The strengths of the composites follow the same trend as the strength of the constituent resin binder material alone (listed in Table 1) in that the silicone resin was the weakest, and the melamine was the strongest by a factor of roughly 3.5. Regardless after an initial period, all variants exhibit a largely elastic-brittle response in this regime.

Figure 4 shows the formation of localized shear in each of the composite variants that appeared during quasi-static compressive loading. In all cases, these regions appeared nearly instantaneously when loading had reached approximately half of the total failure stress. Once formed,

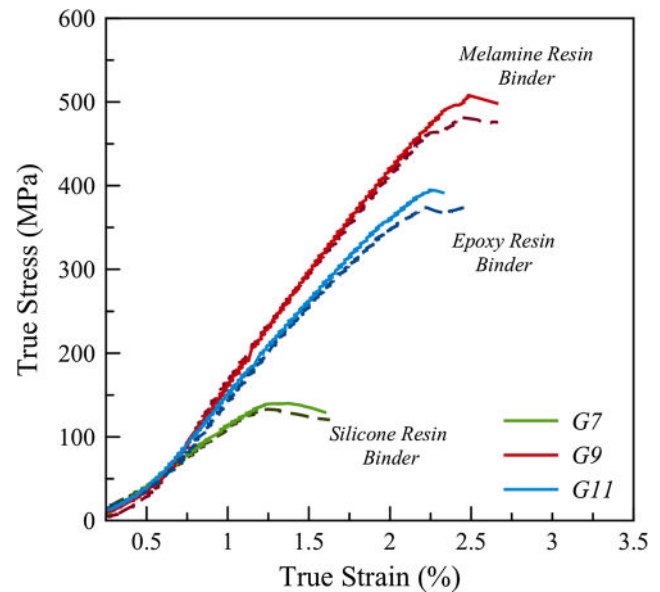


**Fig. 3** Constitutive response of three types of woven glass fiber composites varying in resin binder material loaded quasi-statically

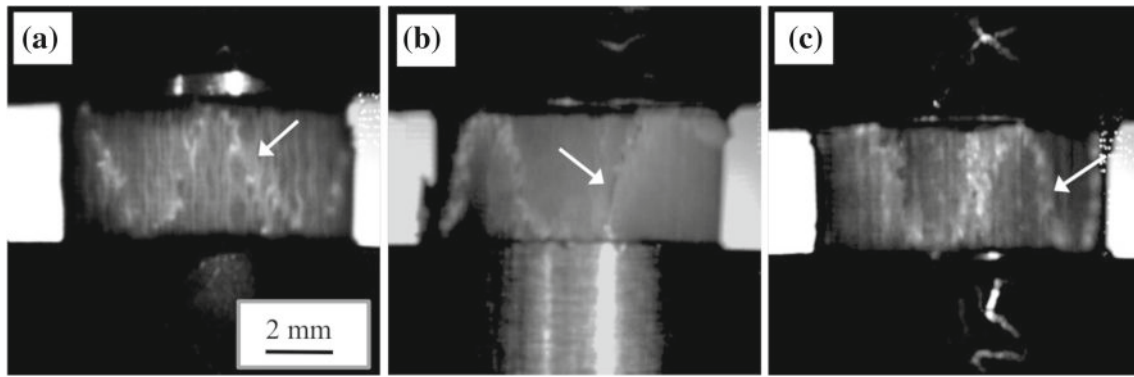


**Fig. 4** Characteristic shear formation highlighted by arrows in the (a) silicone resin binder, (b) epoxy resin binder, and (c) melamine resin binder woven glass fiber composites under quasi-static compressive loading

these light color bands increased only in width and lightness until macroscopic failure. The lighter regions appear to be due to increased specular reflection off of the shear plane as that surface is no longer smooth (due to fiber sliding/stretching and local buckling as discussed in Section “Failure Process”), as well as the exposure of the lighter fiberglass constituent. The failure observed appears to occur along two shear planes in between roughly 40 to 60 degrees relative to the loading axis, and was consistent in angle per resin binder materials tested. Microscopic observation of the fracture plane indicates that similarly orientated fiber yarns fail along the shear plane of adjacent tows.

Dynamic compressive loading produced similar trends in failure strength with resin binder variants, but post-mortem microscopy revealed more dominant fiber pullout along the shear planes. Figure 5 shows characteristic tests for each of the three types of woven glass fiber composites investigated at approximately  $10^3 \text{ s}^{-1}$ . When compared with the quasi-static compressive strength, the silicone resin composites exhibited an increase by a factor of 1.6, the epoxy resin composite by 1.3, and the melamine by 1.2 (showing relatively little rate-dependence). Similar to quasi-static results, all composites had strains around 3%. High-speed imaging shows the matrix material for the epoxy and melamine resin binder composites failing in a brittle manner, both fracturing and ejecting fragments away from the sample. The silicone resin binder composite appeared to have large out-of-plane deformations during loading and no matrix ejection, suggesting a softer response where the elastic-brittle assumptions used in the analysis may be less appropriate, and most likely the strain rate in the sample reached closer to  $10^2 \text{ s}^{-1}$ .

One characteristic result of these composites under dynamic loading is shown in Fig. 6 with a melamine resin binder. Under dynamic loading, all composite variants developed multiple shear formations, or symmetric

cross-shear formations forming visible X's on the sample (instead of single V-shape bands viewed under quasi-static loading). High-speed imaging reveals that these shear formations fully form within 2 to 4 frames, which means the band propagates at an angle across the sample within 8 to 15  $\mu\text{s}$ , corresponding to surface speeds of hundreds of meters per second. At the initial portion of loading (A) there is no surface damage, however by 50% of the loading pulse (B) symmetric light spots are seen in the top half of the sample (and later verified by microscopy to be the initial local kink and buckling of the geometrically similar fiber locations in the weave). Between the next two frames (C and D) the initial shear brands have fully formed across the sample and new light spots in geometrically identical fiber locations are forming where the next bands will evolve. By the late stages (E and F), the material has reached a limit and

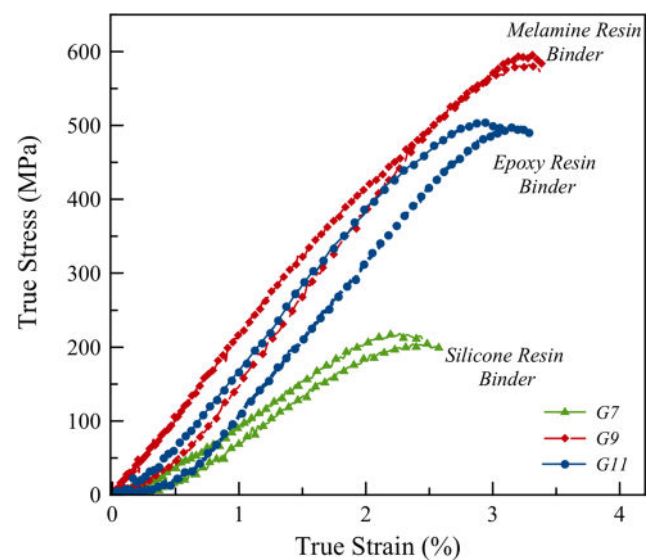


**Fig. 5** Constitutive response of three types of woven glass fiber composites varying in resin binder material loaded dynamically

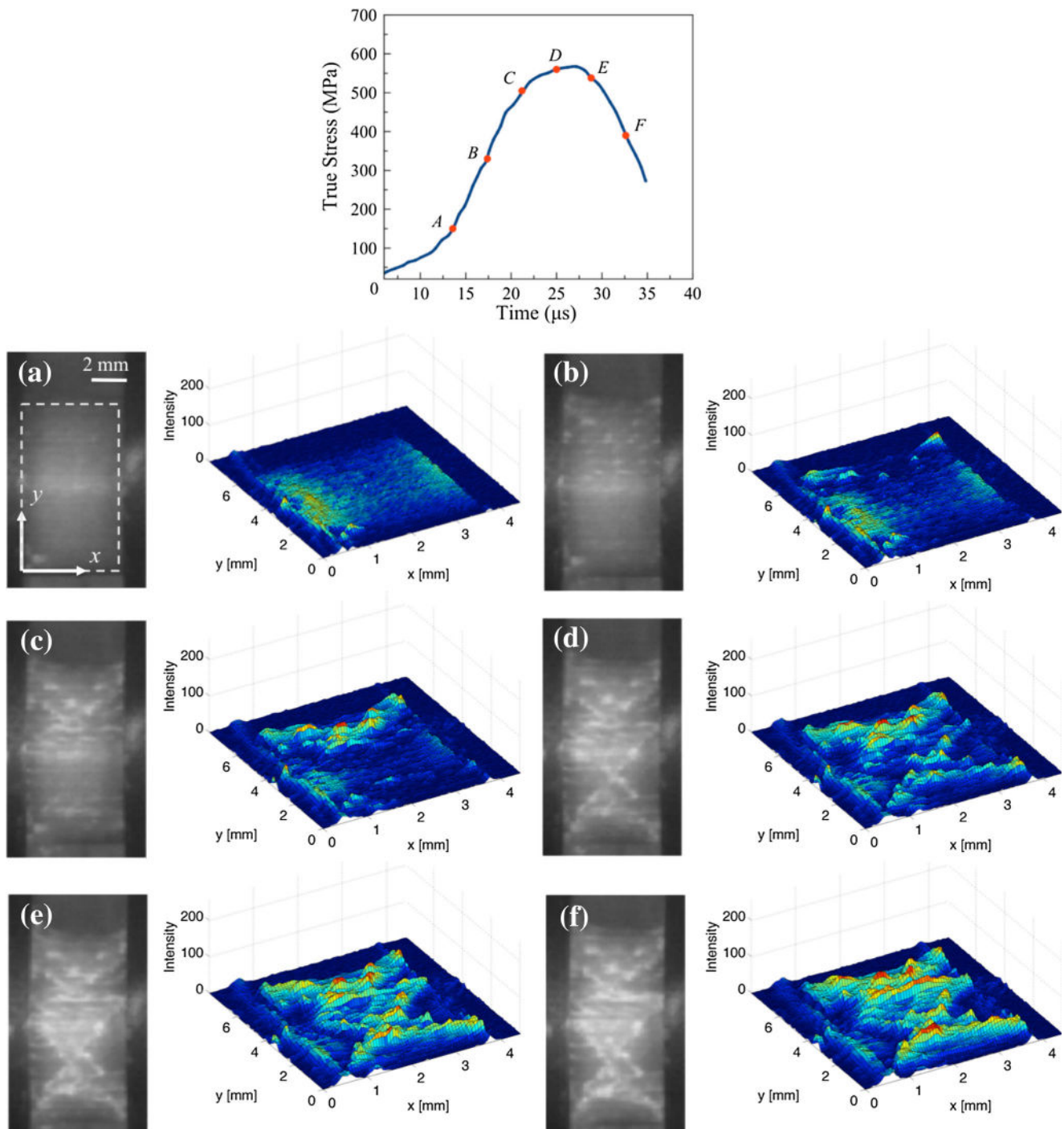


**Fig. 6** Characteristic results shown for a melamine resin binder woven glass fabric composite under dynamic compressive loading with corresponding high-speed images and grayscale light intensity mapping of evolution of shear formation (*dashed line A* shows the specimen outline used for the region of light intensity mapping). The mapped images are shown with an aspect ratio of 1 for visual clarity

damage increases with crushing, debonding, and cracking through the thickness that leads to macroscopic failure. In order to more quantitatively visualize the rate of shear evolution and view its formation without the optical curvature from the high-speed images, grayscale histograms of the image light intensity were mapped onto three-dimensional

space using MATLAB and are shown next to the corresponding high-speed image in Fig. 6. The light intensity at each pixel in the high speed image with coordinates  $x$  and  $y$  at a given time during loading is a grayscale value that can only vary from 0 (black) to 255 (white) in 8-bits. An initial image of light intensity of the undamaged

sample with a known diameter and height is subtracted from each of the subsequent images during loading to maintain a baseline and remove any initial lighting saturations from reflections. As the lighter shear regions form, the region of white (or more light intensity) increases on the sample as the grayscale histogram shifts from black to white. More details for this type of grayscale mapping technique, along with an error and sensitivity analysis can be found in [40].

Post-mortem optical microscopy of the samples shows the characteristic shear formations for each variant and loading rate. Note that the images shown in Fig. 7 are taken after the sample has been carefully removed from the platens in the test rigs, so additional loading from handling, and further fragmenting may have occurred. There are also optical distortions present from the curvature of the sample within the field of view since the imaging plane is focused on the upper most surface. Regardless, all samples exhibit characteristic shear formations between 45 and 65 degrees. The silicone resin binder composites had the largest regions of localized kinking and fiber stretching and sliding (within the shear region) under dynamic loading, whereas the epoxy and melamine resin binder composite exhibited nominally more brittle behavior, with tearing along the shear planes and larger amounts of fiber pullout from buckling in the shear regions. The dynamic loading of

the melamine resin binder composite had the most catastrophically brittle macroscopic failure and collapse, with large portions of the sample fragmenting and crumbling.

An example of the post-mortem microscopy of the shear planes for the silicone resin binder fiberglass is shown in Fig. 8. All three variants exhibited the same behavior, where shear planes had visible angled damage zones or locations of a beginning and end of the shear region as viewed from the loading direction shown in (b). This zone was largest for the silicone resin binder fiberglass perhaps due to its less brittle response in compression than the melamine or epoxy resin binder fiberglass specimens. When examining fragmented shear planes in all three variants, the damaged fragments (those with the fractured plane in the shear band region) had a large amount of fiber breakage and pullout as shown in (d); whereas the flip side of the fragment with the face not in the shear band region was essentially undamaged and had a clean (nearly undeformed) fiber weave as highlighted in (c).

The combined results of woven fiberglass resin binder composites with equivalent loading orientations and findings of this study are shown as a function of strain rate (on a logarithmic scale) in Fig. 9. While the general trend is an increase in compressive strength from quasi-static to dynamic strain rates with the woven fiberglass composites,

**Fig. 7** Post-mortem optical microscopy of quasi-static and dynamically loaded woven glass composites with varying resin binders in compression

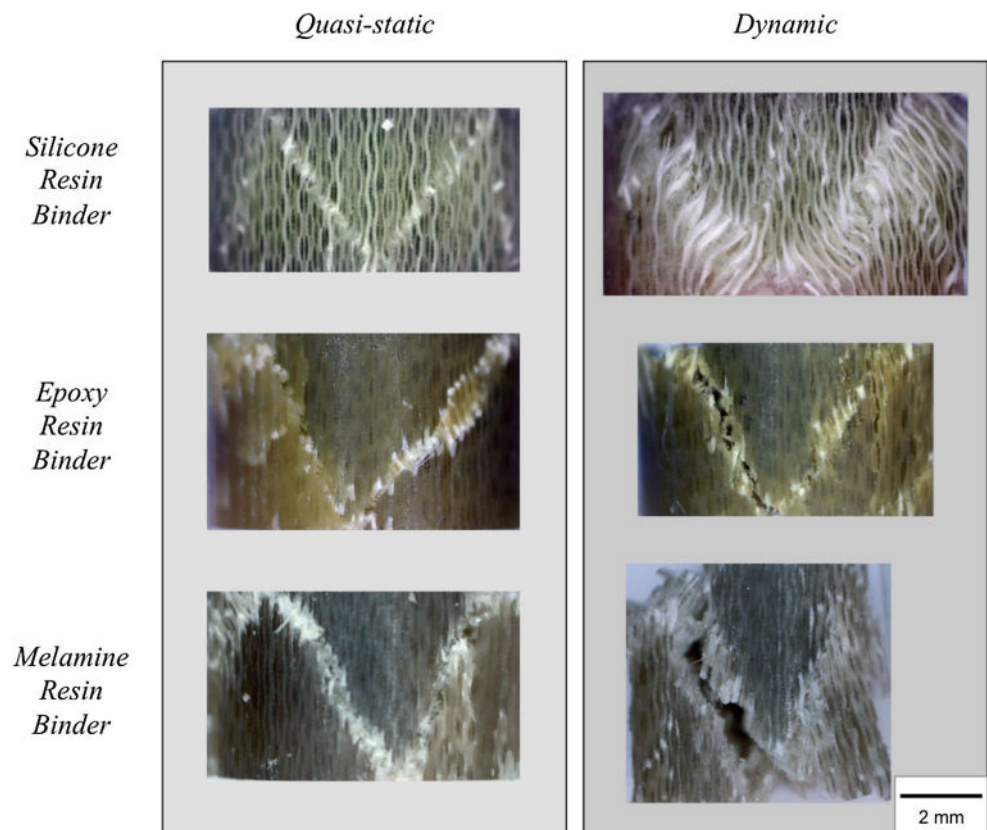
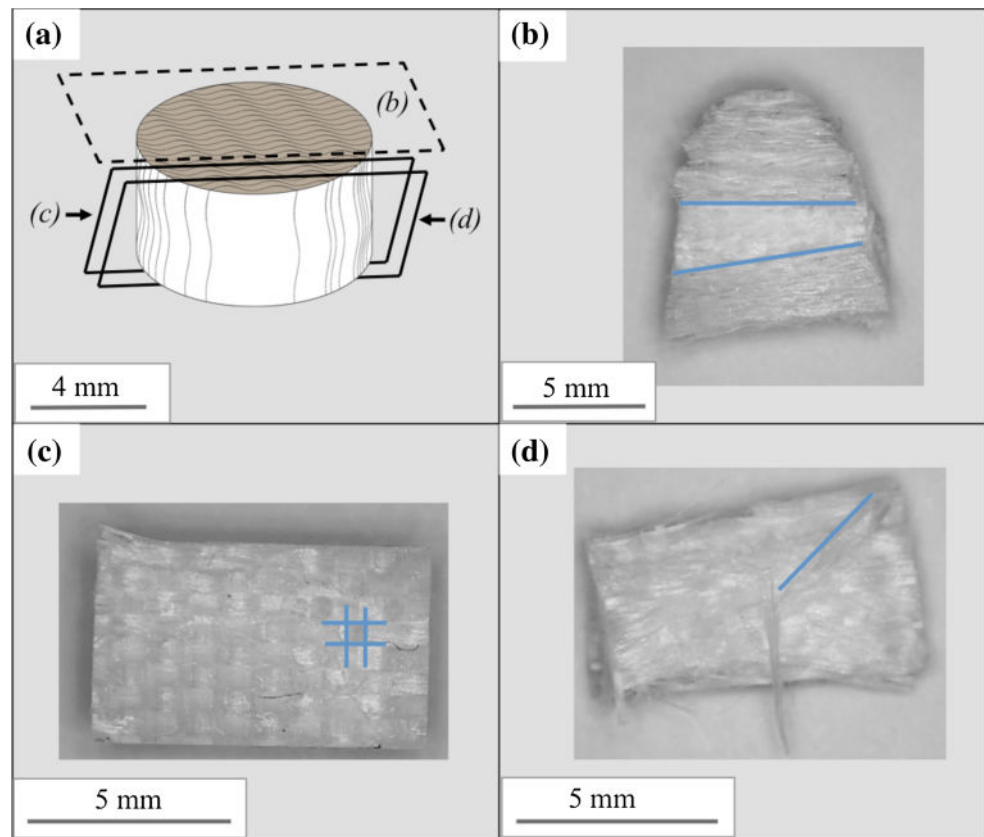


**Fig. 8** (a) Schematic of the fragment planes examined post-mortem via optical microscopy on a silicone resin binder woven glass cloth composite after dynamic compression. Post-mortem microscopy of the resulting fragment (b) as viewed from the loading direction, with blue lines highlighting a region of shear formation where damage accumulates; (c) as viewed from within the cross-section along the shear plane on a fragmented region outside the damage zone with nominally undamaged fiber weave (highlighted by the blue lines); (d) as viewed from within the cross-section along a shear plane on a fragmented region inside the shear region showing large amounts of fiber separation, pullout and breakage and evidence of angled failure propagation (with the direction of failure highlighted by the blue line)



the results do not collapse to master curve due to the difference in composite constituent materials, interpretation of macroscopic failure, potential material preparation differences, and general material variation, to name a few. The data points for all the literature values come from a single test except for the quasi-static value from Ravi-Chandar which is an average of two tests; whereas each data point on the plot from this study is an average of 2 to 3 compression tests with error bars showing the standard deviation [26]. The Nishida et al. and Ravi-Chandar and Satapathy results are from a woven fiberglass epoxy resin binder composite, commercially known as G10, and show large variation in the compressive strength at high rate. However this could be due to the fact that Ravi-Chandar showed a significant drop in the stress-strain response after the maximum compressive strength was achieved, along with post-mortem fragmentation; whereas Nishida et al. reported the maximum elastic response and stated that the specimens were not considered to have fully failed [25, 26]. The Ravi-Chandar and Satapathy results for the quasi-static rate of loading has a large error bar in the horizontal plane as no specific strain rate was provided (thus illustrating the uncertainty). The epoxy fiberglass results in the present study, commercially available G11, fall between the two studies on G10. The Song, Chen and Weerasooriya results are from a woven S-2

glass, SC15 epoxy composite and show a generally stronger response than all the other presented results (with one outlier at a strain rate of  $330 \text{ s}^{-1}$ ) [20]. The increased response in this case is due to the fact that S-2 glass is a higher strength fiber with different mechanical properties than the glass fibers used in the other studies. Of the three matrix variants examined in the present study, all the results were consistent with respect to each other across strain rates, with the silicone resin binder having the weakest response, epoxy the strongest, and the melamine exhibiting the least rate-sensitivity.

### Mohr-Coloumb Analysis

The presence of the localized shear bands in these woven composites suggest that failure could be characterized by a normal stress dependent Mohr-Coulomb type criterion. Measurements of the angles between the failure planes and the loading surface from the tests shown in Figs. 3 and 5 were taken using ImageJ within the focused imaging plane (to avoid optical distortions), with three replications of the same measurement in order to get an average and standard deviation for each sample, and corroborated with the MATLAB results. Using the resulting characteristic angles of the localized regions of shear, failure can be defined to occur

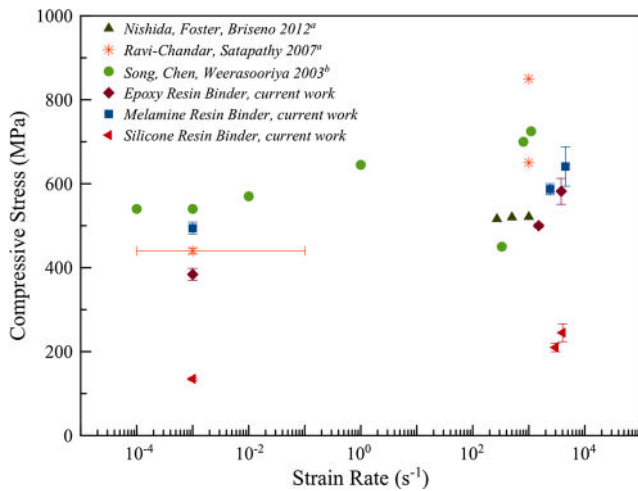


**Fig. 9** Plot illustrating the compressive strength as a function of strain rate on a logarithmic scale for various woven fiberglass resin binder composites with loading orientations the same as the present study. Each data point from literature is from an individual test, except for the quasi-static results from Ravi-Chandar which shows the uncertainty in the strain rate by the horizontal error bar. Each data point on the plot from the present study is an average of 2 to 3 tests with the error bars displaying the standard deviation. <sup>a</sup> Results on commercially available woven fiberglass with epoxy resin (G10) [25, 26], <sup>b</sup> Results from a woven S-2 glass, SC15 epoxy composite [20]

when the shear stress at a particular plane reaches a critical value, and is related to the normal stress acting on the plane by

$$\tau = \tau_0 + \mu\sigma_n \quad (5)$$

where  $\sigma_n$  is the normal stress, and  $\tau$  is the shear stress components acting on the failure plane. The  $\tau_0$  parameter is commonly defined as cohesive shear strength (in the absence of normal stress) and  $\mu$  is a coefficient of internal friction, with compressive stress defined in a positive sense in this case. As depicted in Fig. 10, that the geometric relation between Mohr's circle and the failure line drawn is

$$\mu = \tan \phi = \tan (2\alpha - 90^\circ) \quad (6)$$

where  $\phi$  is a friction angle, and  $\alpha$  is the average orientation of the failure planes. As demonstrated in [21], the cohesive shear strength,  $\tau_0$  and the friction angle are related by

$$\tau_0 = \frac{\sigma_u}{2} \left( \frac{1 - \sin \phi}{\cos \phi} \right) \quad (7)$$

where  $\sigma_u$  is the average compressive strength of the composite.

The results of the Mohr-Coulomb failure analysis are shown in Table 2. The angle of shear localization was found to be nominally consistent per test condition with respect

to the rate of loading and resin binder variant. Out of the three compositions examined, the melamine resin binder woven glass fiber composite did not appear to have rate-influence shear plane formation (at least within the range and type of loading conducted). In the epoxy and silicone resin binder woven fiber composites, the angle of shear formation decreased when loaded dynamically, decreasing the internal friction coefficient  $\mu$ . The melamine resin binder composite also exhibited the least amount of rate dependence on compressive strength in the results presented, which could help explain the nominally identical shear formation angles in quasi-static and dynamic loading. To provide some comparison, Mohr-Coulomb criterion for a typical weak mineral has  $\mu$  less than 0.3 such as brucite [41], and stronger rock values have  $\mu$  of 0.4 to 0.7, like Blair dolomite at Tennessee sandstone [42]. It should be noted that with increasing temperature and/or pressure, the value of  $\mu$  decreases to approach zero in the limit. At constant temperature and strain rate, the Mohr envelope remains consistently concave towards the  $\sigma_n$  axis, and only approaches a horizontal asymptote when the normal stress is high enough. That means, in a fully ductile or plastic condition, the  $\mu$  value becomes nominally zero, as it is in ductile metals. This suggests that the silicone resin binder had the most ductile-like behavior and exhibited the lowest  $\mu$  values, whereas the melamine exhibited rate dependent  $\mu$  values more analogous to a Solenhofen limestone which has little rate dependence in strain rate regimes tested here and similar  $\mu$  values [43]. The Mohr-Coulomb failure model discussed above is utilized in the quasi-static sense, in that only the ultimate compressive strength value changed with strain rate from the experimental measurements, but future work could extend the model by introducing a strain rate dependence in the formulation on the cohesive shear strength term, or  $\tau_0(\dot{\epsilon})$ .

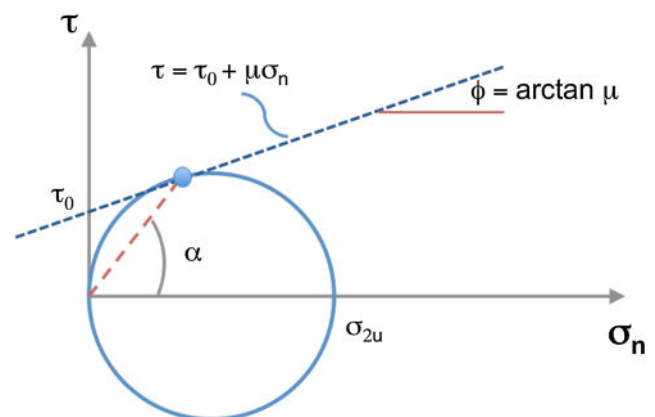


**Fig. 10** Geometric representation of the Mohr-Coulomb failure criterion

**Table 2** Mohr-Coulomb failure analysis on woven glass fiber composites

Resin binder	Quasi-Static			Dynamic		
	$\alpha^*$	$\mu$	$\tau_0$ (MPa)	$\alpha^*$	$\mu$	$\tau_0$ (MPa)
Silicone	$50 \pm 2.8^\circ$	0.17	67	$47 \pm 1.5^\circ$	0.06	100
Epoxy	$61 \pm 2.1^\circ$	0.64	104	$51 \pm 2.8^\circ$	0.20	240
Melamine	$55 \pm 1.2^\circ$	0.35	171	$59 \pm 4.7^\circ$	0.49	157

\*Experimentally measured between failure plane and loading surface.

## Failure Process

Optical microscopy combined with the *in-situ* high-speed images and maps of the shear evolution in compression provide insight on understanding of the shear evolution and ultimate failure process in these woven composites. To that end, an additional Celestron 5 MPa handheld digital microscope was mounted and used to take static images of the samples during quasi-static compression in order to capture magnified early failure onset before full shear band formation. A schematic representation of the failure process, as well as images from the digital microscope are shown in Fig. 11. It should be noted that adiabatic heating of the samples which could dramatically effect matrix behavior does not play a significant role during dynamic testing in this study. Assuming all work done on the samples during loading contributes to adiabatic heating, the adiabatic heat rise can be estimated to equal the product of the maximum force and displacement on the sample, divided by the product of the mass and specific heat (assumed to be on the order of 0.9 kJ/kg-K using rule of mixtures for the constituent materials [34]). With this approximation, the temperature rise was found to be on the order of 10 degrees Celsius. This calculation is corroborated by Song, Chenn and

Weerasooriya's work on S-2 glass/SC15 epoxy woven composite, where they placed a thermocouple inside the sample and measured an approximately 18 degree Celsius rise in temperature in the sample during dynamic compression. Consequently neglecting thermomechanical effects, the fiber yarns that have weave axes along the direction of loading reach a local compressive limit and become unstable, beginning to locally kink and microbuckle. This initial microbuckling is shown in (d) of Fig. 11. At the geometrically identical locations in the weave, the fibers at interlacing junctions are subjected to a shear loading state (due to their angle with respect to the loading plane) and begin to fail and separate, and is shown in (c). As damage begins to locally accumulate, the stress in the sample is redistributed in the undamaged material which causes the matrix to crack near the vicinity of the shear failure planes. This failure mode propagates along the observed shear plane which is influenced by the kink band and buckling formations, and stacking of the tows, as shown in (b). Consequently, the angle of the formation of shear depends on the architecture of the weave and the weave-matrix interface strength. The fiber yarns in the direction perpendicular to the loading plane are subjected to transverse tensile loads which results in fiber matrix debonding,

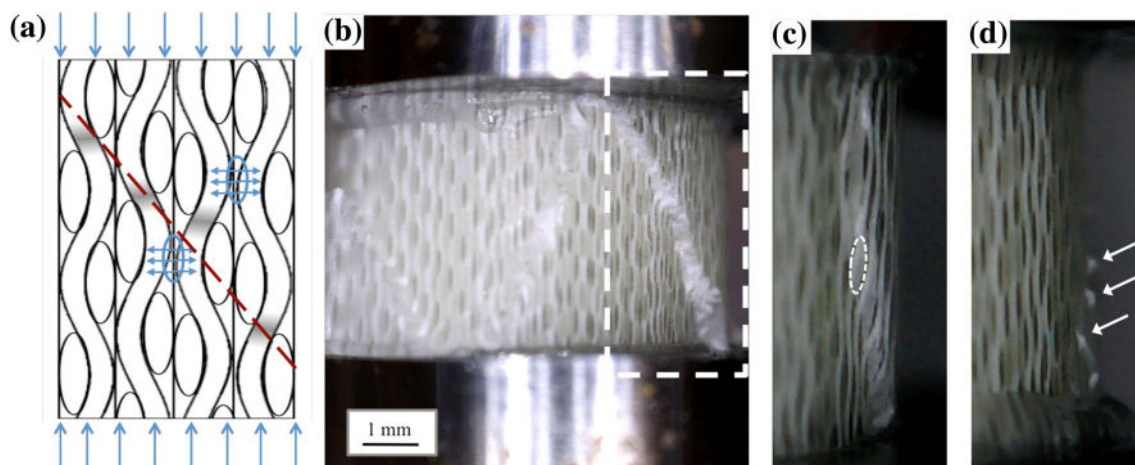


**Fig. 11** (a) Illustration of the compression failure mechanism in woven fiberglass resin binder composites, figure adapted from [22]. (b) Microscopy of the shear formation in woven glass fiber silicone resin binder composite with a callout to show failure process mechanisms of (c) fiber separation and (d) localized microbuckling

leading to microcracks generated both near the loading plane and near the shear failure plain within the fiber yarn. These microcracks coalesce to create macroscopic rapidly propagating failure surfaces where both brittle fracture and delimitation occur, leading to the global failure of the specimen.

## Conclusions

Quasi-static and dynamic compressive testing were conducted on three types of commercially available woven glass fabric composites with varying resin binders of silicone, epoxy, and melamine. The strength and constitutive response are shown at strain rates from  $10^{-3}$  to  $10^3$  s $^{-1}$  where melamine resin binder glass fiber composite exhibited the highest strength by a factor of 3.5 over the silicone resin binder which had the weakest response. Additionally, the melamine resin binder composite showed little rate dependence on failure strength, increasing by a factor of 1.2, whereas the epoxy increased by a factor of 1.3 and the silicone by 1.6. High-speed imaging during loading revealed the sudden formation of shear failure planes. The shear evolution was mapped using grayscale histograms of the light intensity in the shear regions, and the resulting characteristic angles were measured and analyzed in the context of a Mohr-Coulomb failure criterion. These results, along with optical microscopy of the recovered specimens, revealed that initiation appears due to local instabilities from kinking and microbuckling, influenced by the stacking and interlacing regions of tows.

**Acknowledgments** The authors are grateful for support of this work through the Research and Educational Programs at the Ohio Aerospace Institute through the NASA Glenn Research Center Faculty Fellowship Program in 2013, as well as the 2014 Harry C. Bartels Faculty Engineering Development Award at Drexel University.

## References

- Hahn HT, Tsai SW (1973) Nonlinear elastic behavior of unidirectional composite laminae. *J Compos Mater* 7(1):102–118
- Gates TS, Sun CT (1991) Elastic/viscoplastic constitutive model for fiber reinforced thermoplastic composites. *AIAA J* 29(3):457–463
- Harding J (1993) Effect of strain rate and specimen geometry on the compressive strength of woven glass-reinforced epoxy laminates. *Composites* 24(4):323–332
- Yoon KJ, Sun CT (1991) Characterization of elastic-viscoplastic properties of an AS4/PEEK thermoplastic composite. *J Compos Mater* 25(10):1277–1296
- Budiansky B, Fleck NA (1993) Compressive failure of fibre composites. *J Mech Phys Solids* 41(1):183–211
- Takeda N, Wan L (1995) Impact compression damage evolution in unidirectional glass fiber reinforced polymer composites. High strain rate effects on polymer, metal and ceramic matrix composites and other advanced materials, pp 109–113
- Tay TE, Ang HG, Shim VPW (1995) An empirical strain rate-dependent constitutive relationship for glass-fibre reinforced epoxy and pure epoxy. *Compos Struct* 33(4):201–210
- Weeks CA, Sun CT (1998) Modeling non-linear rate-dependent behavior in fiber-reinforced composites. *Compos Sci Technol* 58(3):603–611
- Lee SH, Waas AM (1999) Compressive response and failure of fiber reinforced unidirectional composites. *Int J Fract* 100(3):275–306
- Vogler TJ, Kyriakides S (2001) On the initiation and growth of kink bands in fiber composites: Part I. experiments. *Int J Solids Struct* 38(15):2639–2651
- Xiao JR, Gillespie JW (2007) A phenomenological Mohr-Coulomb failure criterion for composite laminates under interlaminar shear and compression. *J Compos Mater* 41(11):1295–1309
- Harding J (1989) Impact damage in composite materials. *Sci Eng Compos Mater* 1(2):41–68
- Abrate S (1991) Impact on laminated composite materials. *Appl Mech Rev* 44(4):155–90
- Abrate S (1994) Impact on laminated composites: recent advances. *Appl Mech Rev* 47(11):517–544
- Cantwell WJ, Morton J (1991) The impact resistance of composite materials—a review. *Composites* 22(5):347–362
- Kumar P, Garg A, Agarwal BD (1986) Dynamic compressive behaviour of unidirectional GFRP for various fibre orientations. *Mater Lett* 4(2):111–116
- Shokrieh MM, Omidi MJ (2009) Compressive response of glass-fiber reinforced polymeric composites to increasing compressive strain rates. *Compos Struct* 89(4):517–523
- Ochola RO, Marcus K, Nurick GN, Franz T (2004) Mechanical behaviour of glass and carbon fibre reinforced composites at varying strain rates. *Compos Struct* 63(3):455–467
- Staab GH, Gilat A (1995) High strain rate response of angle-ply glass/epoxy laminates. *J Compos Mater* 29(10):1308–1320
- Song B, Chen W, Weerasooriya T (2003) Quasi-static and dynamic compressive behaviors of a S-2 glass/SC15 composite. *J Compos Mater* 37(19):1723–1743
- Vural M, Ravichandran G (2004) Transverse failure in thick S2-glass/epoxy fiber-reinforced composites. *J Compos Mater* 38(7):609–623
- Khan AS, Colak OU, Centala P (2002) Compressive failure strengths and modes of woven S2-glass reinforced polyester due to quasi-static and dynamic loading. *Int J Plast* 18(10):1337–1357
- El-Habak AMA (1991) Mechanical behaviour of woven glass fibre-reinforced composites under impact compression load. *Composites* 22(2):129–134
- Powers BM, Vinson JR, Hall IW, Hubbard RF (1997) High strain rate properties of cycom 5920/1583. *AIAA J* 35(3):553–556
- Nishida EE, Foster JT, Briseno PE (2012) Constant strain rate testing of a G10 laminate composite through optimized kolsky bar pulse shaping techniques. *J Compos Mater* 47(23):2955–2963
- Ravi-Chandar K, Satapathy S (2007) Mechanical properties of G-10 glass-epoxy composite. Defense Technical Information Center
- Harding J, Dong L (1994) Effect of strain rate on the interlaminar shear strength of carbon-fiber-reinforced laminates. *Combust Sci Technol* 51(3):347–358
- Benloulou ISC, Rodriguez J, Martinez MA, Galvez VS (1997) Dynamic tensile testing of aramid and polyethylene fiber composites. *Int J Impact Eng* 19(2):135–146

29. Wang Y, Xia Y (2000) A modified constitutive equation for unidirectional composites under tensile impact and the dynamic tensile properties of kfrp. *Compos Sci Technol* 60(4):591–596
30. Sierakowski RL, Chaturvedi SK (1997) Dynamic loading and characterization of fiber-reinforced composites. Wiley-Interscience, New York
31. Sierakowski RL (1997) Strain rate effects in composites. *Appl Mech Rev* 50(12):741–761
32. Al-Hassani STS, Kaddour AS (1997) Strain rate effects on GRP, KRP and CFRP composite laminates. In: *Key engineering materials*, vol 141. Trans Tech Publ, pp 427–452
33. Greszczuk LB (1982) Damage in composite materials due to low velocity impact. Wiley, New York
34. MatWeb (2014) Material property data. <http://www.matweb.com>
35. Frew DJ, Forrestal MJ, Chen W (2002) Pulse shaping techniques for testing brittle materials with a split hopkinson pressure bar. *Exp Mech* 42(1):93–106
36. Frew DJ, Forrestal MJ, Chen W (2005) Pulse shaping techniques for testing elastic-plastic materials with a split hopkinson pressure bar. *Exp Mech* 45(2):186–195
37. Kolsky H (1949) An investigation of the mechanical properties of materials at very high rates of loading. *Proc Phys Soc London, Sect B* 62(11):676
38. Chen W, Song B (2010) Split Hopkinson (Kolsky) bar: design, testing and applications. Springer Science & Business Media
39. Ramesh KT (2008) High rates and impact experiments. In: *Springer handbook of experimental solid mechanics*. Springer, pp 929–960
40. Lamberson LE, Ramesh KT (2015) Spatial and temporal evolution of dynamic damage in single crystal  $\alpha$ -quartz. *Mech Mater* 87:61–79
41. Moore DE, Lockner DA, Iwata K, Tanaka H, Byerlee JD (2001) How brucite may affect the frictional properties of serpentinite. US Department of the Interior. US Geological Survey
42. Handin J (1969) On the Coulomb-Mohr failure criterion. *J Geophys Res* 74(22):5343–5348
43. Green SJ, Perkins RD et al (1968) Uniaxial compression tests at varying strain rates on three geologic materials. In: *The 10th US symposium on rock mechanics (USRMS)*. American Rock Mechanics Association

